Inorganic Chemistry

Article

pubs.acs.org/IC

Synthesis of Adenine-Modified Reduced Graphene Oxide Nanosheets

Huaqiang Cao,*[,†] Xiaoming Wu,[†,‡] Gui Yin,[‡] and Jamie H. Warner[§]

[†]Department of Chemistry, Tsinghua University, Beijing 100084, P. R. China

[‡]Department of Chemistry, Nanjing University, Nanjing 210093, P. R. China

[§]Department of Materials, University of Oxford, Parks Road, Oxford OX1 3PH, United Kingdom

Supporting Information

ABSTRACT: We report here a facile strategy to synthesize the nanocomposite of adenine-modified reduced graphene oxide (AMG) via reaction between adenine and GOCl which is generated from $SOCl_2$ reacted with graphite oxide (GO). The as-synthesized AMG was characterized by transmission electron microscopy (TEM), atomic force microscopy (AFM), UV−vis absorption spectroscopy, Fourier transform infrared (FT-IR) spectroscopy, Raman spectroscopy, thermogravimetric analysis (TGA), X-ray photoelectron spectroscopy (XPS), cyclic voltammetry (CV), and galvanostatic discharge analysis. The AMG owns about one adenine group per 53 carbon atoms on a graphene sheet, which improves electronic conductivity compared with reduced graphene oxide (RGO). The AMG displays enhanced supercapacitor performance compared with RGO accompanying good stability and good cycling behavior in the supercapacitor.

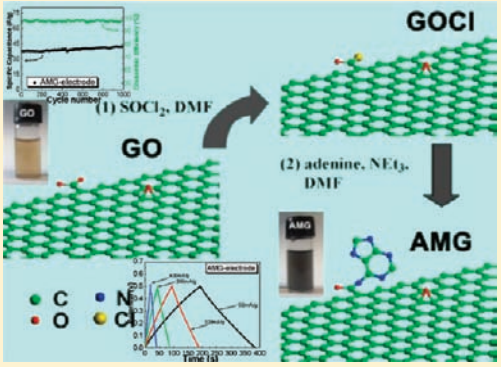

1. INTRODUCTION

Since graphene was obtained by mechanical exfoliation in 2004,[1] it has aroused great interest to synthesize graphene-based materials for various applications, which is the driving force in the field.[2] It is known that graphene-based electronics will not appear in the near future; however, the most immediate applications for graphene are for possible use in composite materials.[2c] Graphene and chemically modified graphene have been synthesized and demonstrated to be promising candidate materials with various applications, such as n-type graphene field-effect transistors,[2b] 'paper-like' materials,[3a] a graphene-based single-bacterium resolution biodevice,[3b] polymer−graphene nanocomposites with mechanical and thermal enhancement,[3c] and inorganic nanoparticles−graphene hybrids used as energy-storage materials,[3d−f] etc. It is worth pointing out that the functional groups covalently attached in graphite oxide (GO) or reduced graphene oxide (RGO) sheets will reduce the interplane forces and impact the hydrophobic character, promoting complete exfoliation of GO or RGO layers in aqueous media.[4] Nanostructured materials with unusual electrical and mechanical properties have been applied in advanced energy conversion and storage devices.[5] Carbonaceous materials such as graphene-based materials could be a promising alternative as electrode materials in energy-storage devices because these materials have excellent electrical conductivity, large surface area, and chemical stability.[6] With this motivation, we report, for the first time, a simple approach for synthesizing chemical modification graphene−adenine-modified graphene (termed as AMG).

2. EXPERIMENTAL SECTION

Synthesis of Graphene Oxide (GO). We synthesized water-soluble single-layer GO by a modified Hummer's method[7] from graphite powders (chemically pure, CP) as reported in great detail elsewhere.[8] First, 3 g of graphite powder was added to 69 mL of concentrated H_2SO_4 with stirring in an ice bath, followed by adding 1.5 g of $NaNO_3$ into the mixture. The mixture was continuously stirred, while 9 g of $KMnO_4$ was added slowly while keeping the temperature of the mixture below 20 °C. Then, the mixture was kept at 35 °C for 30 min, followed by adding 137 mL of deionized water. After the mixture was stirred for a further 15 min continuously, 420 mL of deionized water and 10 mL of an aqueous solution of 30 wt % H_2O_2 was added. The oxidized material was then washed with 1:10 (in volume) HCl solution one time and deionized water three times to remove metal ions and other impurities with centrifugation. The collected material was dried in an oven at 45 °C to obtain brown GO powder. Reduced graphene oxide (RGO) for comparison was also synthesized from GO through reaction with $NaBH_4$ at 80 °C for 3 h, washed with deionized water 3 times, and then dried at 80 °C for 4 h.

Preparation of Adenine-Modified Graphene (AMG). An 80 mg amount of GO was dispersed and refluxed in $SOCl_2$ (20 mL) in the presence of *N*,*N*-dimethyl formaide (DMF) (0.5 mL) at 70 °C for 24 h. At the end of the reaction, excess $SOCl_2$ and solvent were removed by distillation and dried GOCl powder was collected immediately.[9] Then 30 mg of as-synthesized GOCl was allowed to react with 120 mg of adenine powder in 20 mL of DMF in the presence of 0.5 mL of triethylamine at 130 °C for 72 h in nitrogen to obtain AMG. AMG was further washed with HCl solution (0.5 mmol·

Received: October 15, 2011
Published: February 22, 2012

L^{-1}) one time and deionized water three times and dried at 45 °C. RGO was synthesized through a common method.

Characterization. UV−vis absorption spectra were recorded on a UV-2012 spectrophotometer, UNICO. Fourier transform infrared (FT-IR) spectra were obtained on a Nicolet 560 Fourier transform infrared spectrophotometer. Raman spectra (Renishaw, RM 1000) were measured with excitation from the 514.5 nm line of an Ar-ion laser with a power of about 5 mW at room temperature. X-ray photoelectron spectroscopy (XPS) was carried out on a PHI quantoera SXM with an Al Kα = 280.00 eV excitation source, where binding energies were calibrated by referencing the C1s peak (284.8 eV) to reduce the sample charge effect. Transmission electron microscopy (TEM) was performed using a JEOL 4000HR transmission electron microscope operating at 80 kV. For atomic force microscopy (AFM) measurement, GO or AMG was coated on a mica surface and studies were performed using a Digital Instruments Dimension 3100 microscope in tapping mode. Thermogravimetric analysis (TGA) was carried out on a TGA Q5000 V3.5 Build 252 by heating under a nitrogen atmosphere to 900 °C at a rate of 10 °C·min^{-1}. Electrical conductivity was measured on a Keithley Instruments (Cleveland) conductivity meter using a four-probe head at room temperature.

Electrochemcial Measurement. Cyclic voltammetry (CV) measurements were performed using a CHI 660B electrochemical analyzer interfaced to a computer system with corresponding electrochemical software. The electrode was loaded with 25 mg of samples and tested in the potential range of 0−0.5 V, and the galvanostatic charge/discharge curves were performed at current densities of 50, 100, 200, and 400 mA·g^{-1}.

3. RESULTS AND DISCUSSION

Figure 1 outlines the process for synthesizing the AMG composite. GO was produced by Hummer's method[7] through

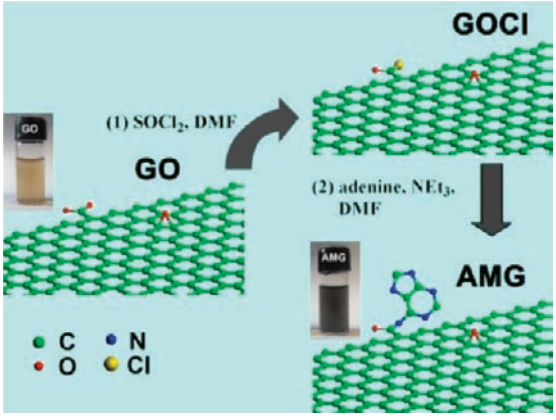

Figure 1. Synthesis of AMG from GO. (Inset) Images of 0.25 mg/mL of GO and AMG dispersion of water.

aicd oxidation of flake graphite, followed by activating carbonyl groups using $SOCl_2$ to lead to formation of −COCl groups at the edge of GO (termed as GOCl). The $-NH_2$ group in adenine ($C_5H_5N_5$, 6-aminopurine, $NH_2-C_5H_3N_4$) can react with −COCl generated from −COOH at the edge of GO in the presence of DMF which leads to formation of adenine-modified graphene (i.e., AMG). Successful synthesis will be demonstrated by TEM, AFM, UV−vis, FT-IR, Raman, TGA, and XPS tools. Through this chemical modification process of GO the bright yellow GO was converted to black AMG as shown in the inset images of Figure 1. It has been demonstrated that the reduction from GO to RGO is limited to ca. 70% using Hummer's method,[7] which means there is still ca. 30% oxygenated defects existing in RGO,[10] including the epoxide, hydroxyl, carbonyl, and carboxyl both at the edges and in the basal plane.[11] However, the carboxylic (−COOH) and hydroxyl (−OH) groups are most likely at the edges; furthermore, it has been demonstrated that formation of the carbon−nitrogen bond should occur mostly at the edge of the graphene where chemical reactivity is high.[2b] Thus, the edge-functionalized graphene between RGO and adenine after $SOCl_2$ activation of the COOH groups was applied to functionalize RGO.

TEM and AFM images of GO and AMG are presented in Figure 2. Large GO and AMG sheets were observed on the

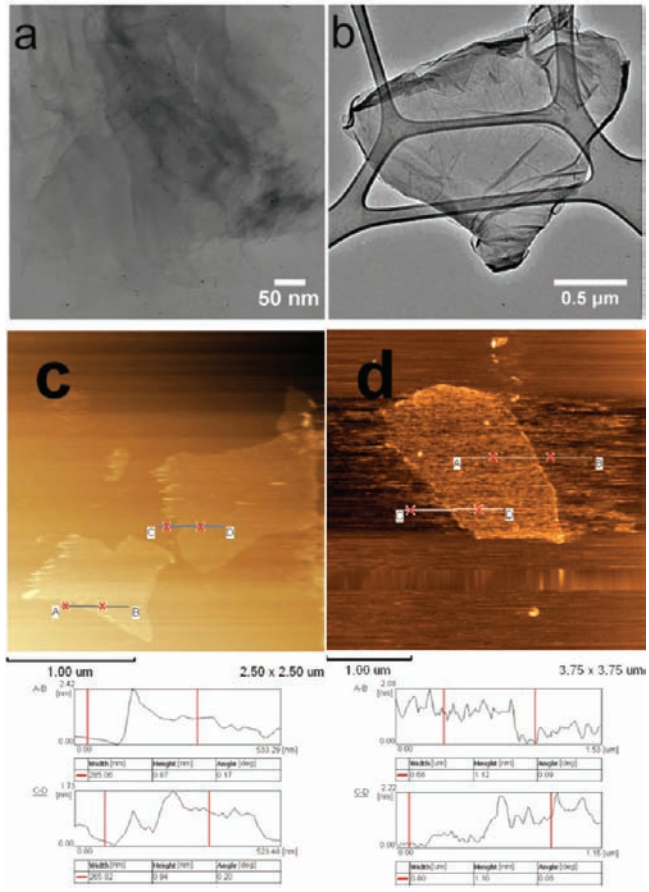

Figure 2. TEM images of (a) GO and (b) AMG and tapping AFM images of (c) GO and (d) AMG on mica.

TEM grid (Figure 2a and 2b). The sheets typically appeared crumpled with lots of folds that are indicative of the ultrathin nature of the sheets. AFM is another direct method to observe the degree of exfoliation of graphene sheets and chemical modification of the surface. Representative AFM images of GO and AMG sheets in tapping mode are shown in Figure 2c and 2d, respectively, with the samples deposited onto a mica flake surface from an aqueous dispersion of 0.1 mg·mL^{-1}. Figure 2c shows that the average thickness of single GO sheets is ∼0.91 nm, which leads to the conclusion that exfoliation of precursor GO has been completed. As presented in Figure 2d, the AMG sheets self-assemble to form folds, which lead to a thickness of ∼1.1 nm.

Figure 3a illustrates the UV−vis absorption spectra of AMG, GO, and adenine in water. Absorption of GO includes two typical features, i.e., a peak at 236 nm corresponding to the $\pi-\pi^*$ of C═C and a shoulder at 290−300 nm due to $n-\pi^*$

dx.doi.org/10.1021/ic2022402 | Inorg. Chem. 2012, 51, 2954−2960

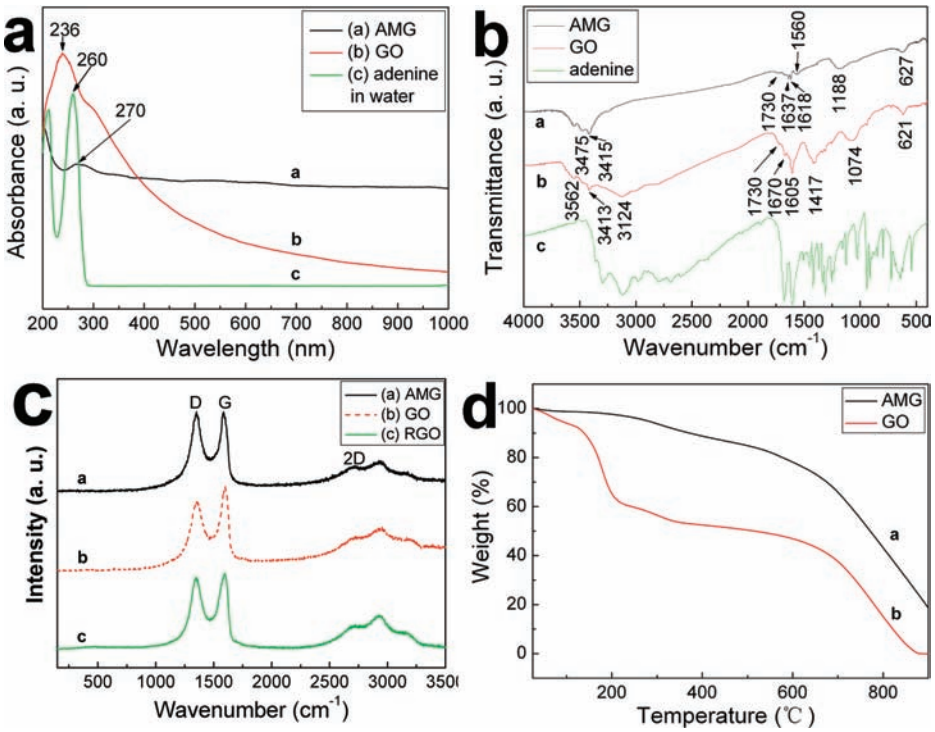

Figure 3. (a) UV−vis spectra of (curve a) AMG, (curve b) GO, and (curve c) adenine dispersed in deionized water. (b) FT-IR spectra of (curve a) AMG, (curve b) GO, and (curve c) adenine. (c) Raman spectra of (curve a) AMG, (curve b) GO, and (curve c) RGO. (d) TGA pattern of (curve a) AMG and (curve b) GO in N_2.

transition of the C═O bond.[12] Adenine shows a sharp peak centered at 260 nm, while AMG exhibits a broad peak at around 270 nm with a red shift of 34 nm to the corresponding peak of GO. These results indicate that the forming bonds with the adenine moiety have perturbed the electronic state of GO in the ground state.[13]

Evidence of successful functionalization following covalent coupling of adenine on RGO can be further demonstrated by FT-IR spectra (Figure 3b). The FT-IR spectrum of GO shows a C−O stretch at ∼1074 cm^{-1} and a broad O−H stretch at 3100−3600 cm^{-1} as well as a C═O stretch at 1730 cm^{-1}, which is in accord with previous reports.[14] However, in the spectrum of AMG, the peak at 1730 cm^{-1} almost disappears and the peak emerging at 1637 cm^{-1} is characteristic of the C═O stretch in the amide group,[13] which cannot be found in the spectrum of GO. Stretching of the amide C−N appears as a strong peak at 1188 cm^{-1}. The peaks at 1560 and 1618 cm^{-1} are attributed to the graphene vibration.[15] The peak at 3415 cm^{-1} is attributed to N−H stretching. These results demonstrate that adenine molecules were covalently bonded to GO by the amide linkage.

Raman spectroscopy is an important tool for analysis of graphite-like materials such as carbon nanotubes and graphene.[16] The strong Raman response for graphene can be regarded as the enhanced resonant by C−C π states, while the Raman response for disordered carbon-based materials will decrease. The main features in the Raman spectrum of AMG are the D and G peaks that lie at about 1350 and 1583 cm^{-1}, respectively (Figure 3c).[16b] The D peak corresponds to a disorder-induced Raman mode and is associated with the TO (transverse optical) branch near the **K**-point in the Brillouin zone, due to breathing modes in C−C ring structures, which can indicate the amount of disorder in graphene via its intensity.[17] The G mode is due to the doubly degenerate zone center symmetry-allowed E_{2g} mode at the Γ point at the Brillouin zone center,[18] which is assigned to $C(sp^2)-C(sp^2)$ bond stretching vibrations. The G position of AMG is ca. 3 cm^{-1} higher than monolayer graphene (1580 cm^{-1}).[16b] This upshift is partially due to chemical doping, i.e., functionalization.[18] It has been demonstrated that the G mode had a lower frequency shift caused by electron donor dopants while a higher frequency shift was caused by acceptor dopants.[19] It is worth pointing out that the position of the Raman G mode in mechanically exfoliated single-layer graphene varies from 1582 to 1594 cm^{-1}.[17] That means AMG is a functionalized single-layer graphene. The Raman I_D/I_G ratio (where I_D and I_G are the D-peak and G-peak Raman intensities, respectively) is widely used to evaluate the quality of graphene and graphene-based materials.[20] The ratio is a measure of the disorder in the sample, which can be edges, ripples, or any other defects, such as doping organic functions in graphene. From the Raman spectrum obtained using 514 nm laser excitation of AMG, an approximate I_D/I_G of 1.0 can be calculated, compared with I_D/I_G of GO which is about 0.84, and I_D/I_G of RGO which is about 0.96. The I_D/I_G of RGO proved to be larger than that of GO, which is corresponding to the literature.[21] In addition,the I_D/I_G ratio of AMG increases in comparison with that of starting material, implying the functionalization process of graphene skeleton has introduced an amount of structural disorder in the graphene lattice, which also demonstrates that GO has been chemically modified with adenine molecules. The second-order Raman scattering 2D peak of AMG appears at around 2704 cm^{-1}, which is sensitive to the number of layers of graphene.[18,22,23] The 2D mode in graphene is regarded as having two phonons with opposite momentum in the highest optical branch near **K** in the Brillouin zone.[18] It should point out that Raman spectroscopy can clearly distinguish a single layer from a bilayer from few (less than 5) layers according to

dx.doi.org/10.1021/ic2022402 | Inorg. Chem. 2012, 51, 2954−2960

the position and shape of the 2D peak, while AFM has been regarded as, so far, the only method to identify single and a few layers with the limitation of low throughput.[16c,23] We analyzed the layer thickness of the AMG via AFM (Figure 2c and 2d); however, analysis of the Raman 2D mode of AMG will further aid in understanding the layer information of AMG, due to the diameter of the laser spot focused on the sample being ca. 1 μm, larger than the area for AFM analysis. It has been demonstrated by theoretical and experimental data that the position of the 2D peak is predicated to decrease for an increasing electron concentration in doped graphene.[24] Thus, the adenine ring, as acceptor dopant in AMG, can induce the 24 or 5 cm^{-1} upshift of the 2D peak of AMG (ca. 2704 cm^{-1}) with respect to monolayer graphene (2680 cm^{-1})[16b] or mechanically exfoliated single-layer graphene (2699 cm^{-1}).[17] This further demonstrates successful functionalization of graphene into the AMG. The other Raman modes can be observed at 2937 cm^{-1} (D+G mode) and 3190 (2D′ mode) cm^{-1}.[17]

The presence of functional groups on the graphene sheets was further analyzed using TGA by heating under a nitrogen atmosphere to 900 °C at a rate of 10 °C·min^{-1} compared with precursor GO (Figure 3d). The TGA pattern of GO under nitrogen reveals two evident mass losses, which agrees with previous reports.[25] The first one appears as a sharp mass loss at an onset temperature before 200 °C, which can be assigned to decomposition of the oxygen-containing groups in GO structure,[26] while the second mass loss begins approximately at 670 °C due to most of the oxygen-containing functional groups being removed from the GO.[27] By comparison, the TGA pattern of the as-synthesized AMG shows a slight weight loss of about 24.7% until the temperature reaches 670 °C. These results indicate that the oxygen-based groups in GO have formed heat-stable structures via covalent bonding with the adenine moieties.

To further assess the degree of functionalization of the AMG, XPS analysis was carried out (Figure 4). Elemental composition

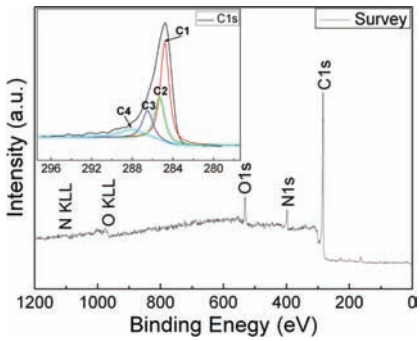

Figure 4. XPS survey scan of AMG. (Inset) C1s photoelectron spectrum.

analysis shows the contents of C, N, and O atoms in AMG are 84.55, 7.23, and 8.22 atomic %, respectively, without counting H atoms. On the basis of these data, it is estimated that there is one adenine group per 53 carbon atoms on a graphene sheet, i.e., about 17.5 wt % of adenine in AMG hybrid nanosheets, which is close to the above TGA weight loss of the adenine group without considering the oxygen-containing functional groups removal. The XPS spectra also reveal that the main peak C1s is located at around 285 eV, which is attributed mainly to sp^2-hybridized graphitic carbon.[26,27] More information can be obtained from XPS spectra in the C1s region. C1s can be divided into four peaks: C1, C2, C3, and C4. The main peak C1 is located at a binding energy of 284.4 eV with peak area proportion of 48.0%, which is attributed to C−C bonding (sp^2 carbon) in defect-free graphite lattice. Peak C2 located at 285.3 eV with a peak area proportion of 23.3% is attributed to carbon in the C−C bonding in defect graphite lattice and C−N sp^2 bonding.[17] The considerable presence of C2 demonstrates the defect structure and formation of an amide bond between the graphene and the adenine. Peak C3 located at a bonding energy of 286.5 eV with a peak area proportion of 16.5% is attributed to carbon in C−O bonding.[27] Peak C4 located at 288.0 eV with a peak area proportion of 12.3% is attributed to carbon in a C═O amide bond.[28] Deconvolution of the peaks of N1s in the XPS spectrum of AMG clearly indicated that the peaks of nitrogen functionalities appeared at 398.95 [characteristic of the imine nitrogen, −N═],[29] 401.08 [characteristic of N bound to the carbonyl C, i.e., NH−C═O],[30] and 405.61 eV [characteristic of general transitions from the N1s core level to the C−N σ^* state][31] (Figure S1a, Supporting Information). The deconvolution peaks of the O1s spectrum were observed at 532.0, 532.3, and 538.8 eV, respectively. The first two peaks can be assigned to the oxygen bound to C by the double bond (C═O from carbonxyl groups linked to aromatic rings) and oxygen singly bound to sp^2 C,[32] and the other peak is attributed to H_2O (Figure S1b, Supporting Information).[33]

The electrical conductivity of the as-synthesized AMG was studied on a Keithley Instruments (Cleveland) conductivity meter using a four-probe head at room temperature. In control, the electrical conductivity of RGO was also measured in the same procedure. Conventional electrical conductors are ruled by Ohm's law

$$G = I/V = \sigma \times L/A \quad (1)$$

where G is the electrical conductance, I the electrical current, V the applied voltage, σ electrical conductivity (a material-dependent property), L the length of a material, and A the cross-section of a material. The electrical conductivity of AMG is ∼429 S·m^{-1}, almost 4.76 times of that of RGO (∼90 S·m^{-1}) (Figure 5). Similar phenomena have been reported. Shi and co-

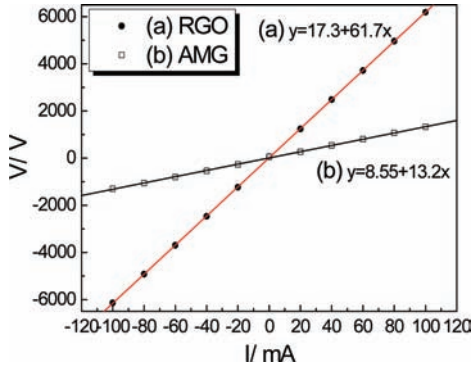

Figure 5. I−V curves of (a) AMG and (b) RGO sheets obtained through a four-probe method.

workers reported the conductivity of 1-pyrenebutyrate-functionalized graphene (PB^-−G) film to be 200 S·m^{-1}, almost 7 orders of magnitude larger than that of a GO film (6×10^{-5} S·m^{-1}) prepared by the same procedure.[34]

It is known that carbonaceous materials are remarkably prevalent for making electrodes used in supercapacitors besides

dx.doi.org/10.1021/ic2022402 | Inorg. Chem. 2012, 51, 2954−2960

fuel cells, due to their large surface area and high conductivity.[35−37] Herein, we focus on application in a supercapacitor of hybrid AMG carbonaceous material. The CV is an effective qualitative and semiquantitative analytical method for studying the electrochemical properties,[38] while the galvanostatic charge−discharge method is a direct means to evaluate the adaptability of supercapacitors.[39] The CV curves of the AMG-, RGO-, and adenine-modified foam nickel electrodes are obtained in 3 M KOH solution at a scan rate of 100 mV·s^{-1} at room temperature. The CV curves of RGO- and AMG-modified foam nickel electrode shows elliptical curves, indicating a faradaic reaction at the interface of electrodes with electrolyte ions, which is a typical behavior of pseudocapacitors (Figure 6).[40] The current of the AMG

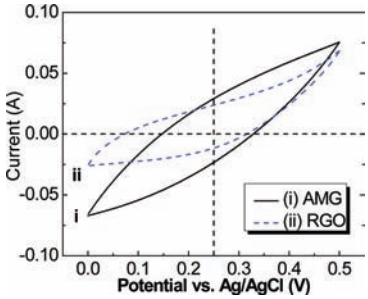

Figure 6. Cyclic voltammograms in supercapacitor of electrodes loaded with (i) 25 mg of AMG and (ii) 25 mg of RGO in the voltage range from 0 to 0.5 V in 3 M KOH aqueous solution at a scan rate of 100 mV·s^{-1} in a supercapacitor.

electrode increases more quickly than that of the RGO electrode as the potential increases, suggesting that the electric conductivity of AMG is better than that of RGO. The AMG-modified electrode has the bigger area of the CV and a higher current value at 0.25 V, the midpoint of the applied voltage, than those of the RGO-modified electrode, which indicates the better capacitive behavior of AMG material. However, the adenine-modified electrode shows a weak cathodic peak (reduction peak) at ∼0.50 V and a corresponding anodic peak at ∼0.32 V vs saturated calomel electrode (SCE) (Figure S2, Supporting Information). However, the redox peaks disappear in the CV curve of AMG. The control experiment of the CV curve of adenine-modified electrode indicates that adenine is indeed chemically inert.[41]

Specific capacitance values can be obtained from the galvanostatic discharge curves (Figure 7a) using the formula as follows[42]

$$C_m = 2 \times I/[(\Delta E/\Delta t) \times m] \quad (2)$$

where C_m is the specific capacitance of the supercapacitor (F·g^{-1}), I is the current of the charge−discharge, $\Delta E/\Delta t$ is the average slope of the discharge curve in the potential range ΔE, Δt is the discharging time period in seconds, m is the mass load of active materials (including positive and negative electrode), and the factor of 2 comes from the fact the total capacitance measurement from the test cells in the sum of two equivalent single-electrode capacitors in series. The average specific capacitance values of AMG-modified electrode are 38.6, 37.6, 35.4, and 33 F·g^{-1}, while they are 23.4, 19, 15, and 11.2 F·g^{-1} for RGO-modified electrode, corresponding to discharge currents of 50, 100, 200, and 400 mA·g^{-1}, respectively (Figure 7a). Interestingly, we can observe the increase of specific capacitance over the first 50 cycles. This phenomenon has also been observed for α-Co(OH)$_2$ long nanowire arrays grown on graphite as the anode material,[43] polyaniline/sodium alginate nanofiber network for supercapacitors,[44] single-walled carbon nanotubes@porous CuO nanobelts as pseudocapacitor electrodes,[45] NiO−TiO$_2$ nanotube as pseudocapacitor electrodes,[46] hierarchical porous NiO nano/microspherical superstructures as supercapacitor electrodes showing an increase during first 300 cycles,[47] hierarchically porous NiO film as an electrochemical pseudocapacitor material even presenting an increase

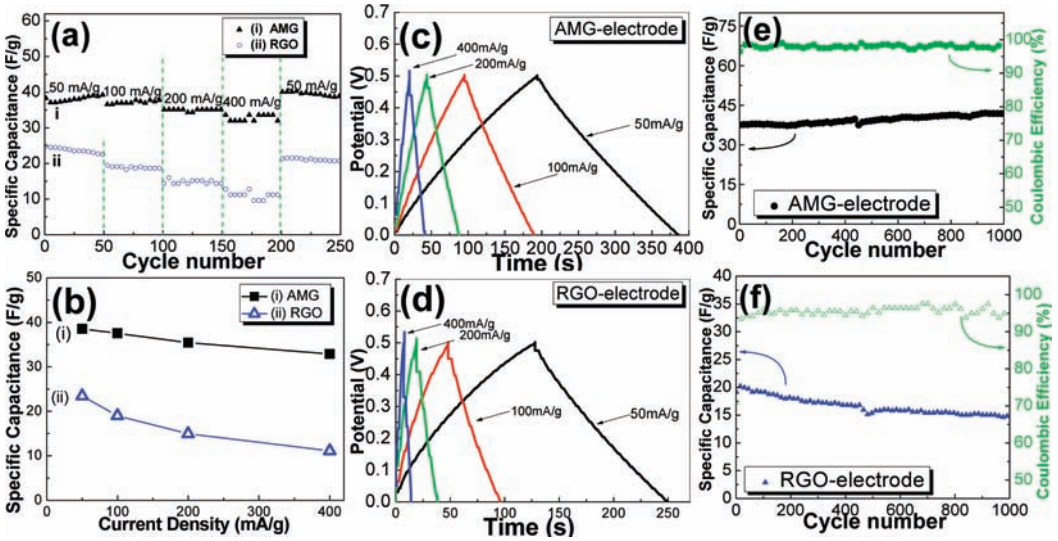

Figure 7. (a) Variation of discharge-specific capacitance in a supercapacitor of electrodes loaded with (i) 25 mg of AMG and (ii) 25 mg of RGO at stepwise increasing current density of 50, 100, 200, 400, and 50 mA/g in 3 M KOH aqueous solution in the voltage range from 0 to 0.5 V. (b) Dependence of the discharge capacitance values (i) AMG and (ii) RGO vs current densities of 50, 100, 200, and 400 mA g^{-1}. Galvanostatic charge/discharging behavior in supercapacitor of electrodes loaded with (c) 25 mg of AMG and (d) 25 mg of RGO in a single cycle under a current density of 50, 100, 200, and 400 mA·g^{-1}. Cyclic performance in a supercapacitor of the discharge-specific capacitance and efficiency of electrode loaded with (e) 25 mg of AMG and (f) 25 mg of RGO under a current density of 50 mA·g^{-1} in the voltage range from 0 to 0.5 V.

dx.doi.org/10.1021/ic2022402 | Inorg. Chem. 2012, 51, 2954−2960

up to the first 500 cycles,[48] and nickel cobaltite aerogel as a supercapacitor material showing an increase up to the first 500 cycles.[49] This phenomenon can be attributed to the fact that the AMG hybrid nanocomposite cannot provide numerous fast electron-transport access to the current collector, restraining quick electron transfer from active redox sites to the electrode during the first 50 cycles. Obviously, the additional first 50 cycles were needed to fully activate the present AMG sample. Noticeably, when the current density returns to the initial 50 $mA{\cdot}g^{-1}$ in the range of 201−250 cycles, a stable high averaged specific capacitance of 39.5 $F{\cdot}g^{-1}$ can be recovered, which means the AMG material has good stability. Compared with initial cycles, there is no capacitance decrease appearing over 200 cycles but a slight 2.3% increase in capacity. The good capacity retention could be attributed to the strong adhesion between AMG and foam Ni substrate. The architecture of AMG is favorable of the electorn-transport accessing the current collector.[43] Another reason for this phenomenon can be attributed to the AMG electrode not fully marinating in the electrolyte solution at initial charge/discharge processes. The AMG electrode soakage degree will increase for the AMG electrode in electrolyte solution accompanying the charge/discharge processes, which will lead to the increase of capacity.[50] Huang and co-workers observed a similar phenomenon, i.e., α-$Co(OH)_2$ nanowire arrays have an average capacity of 436 $F{\cdot}g^{-1}$ after 3000 cycles by decreasing the current rate from 20 to 3 $A{\cdot}g^{-1}$ which is larger than that of 430 $F{\cdot}g^{-1}$ at the initial measued current rate of 3 $A{\cdot}g^{-1}$.[43] Cheng and co-workers reported the graphene/polyaniline composite paper (GPCP) flexible supercapacitors exhibit good cycling stability with an increased retention ratio during the 1400 cycles.[51] As the current density increased, there is a decrease in specific capacitance for both of the electrodes (Figure 7b). Figure 7c and 7d shows the charge−discharge profiles of the AMG- and RGO-modified electrode (the weight of the sample is 25 mg) at various current densities of 50, 100, 200, and 400 $mA{\cdot}g^{-1}$. A nearly linear variation of the voltage is observed during the charging−discharging process; however, an initial voltage drop can be observed, which can be attributed to electrode resistance. This demonstrates that the hybrid supercapacitor made by carbonaceous material−AMG has good electrochemical capacitance performance, and AMG electrode has a larger capacity than that of RGO electrode under the same measured conditions, which is attributed to the higher electrical conductivity of AMG than that of RGO (Figure 5). The cycle life of the supercapacitors was studied at a current density of 50 $mA{\cdot}g^{-1}$. The specific capacitance of AMG or RGO as a function of cycle number cycled between 0 and 0.5 V is shown in Figure 7e and 7f. The obtained AMG electrode shows good cycling behavior with no obvious loss during 1000 cycles with a Coulombic efficiency of 97% of the initial capacitance (Figure 7e), while the RGO electrode exhibits a capacitance retention of lower than 76% of initial capacitance with a decreasing trend (Figure 7f). This indicates the high stability of AMG is suitable for high-performance supercapacitor applications. The AMG-specific capacitance of 39.5 $F{\cdot}g^{-1}$ is about 2.45 times larger than that of puried multiwalled carbon nanotubes (MWNTs) (16.1 $F{\cdot}g^{-1}$)[52] as well as 1.23 times of poly(3,4-ethylenedioxythiophene) (PEDOT, 32 $F{\cdot}g^{-1}$) and 1.46 times of its derivative (27 $F{\cdot}g^{-1}$).[53] However, it is lower than that of single-walled carbon nanotubes (SWNTs) (54 $F{\cdot}g^{-1}$; ∼73.1% of 54 $F{\cdot}g^{-1}$).[42]

4. CONCLUSIONS

In summary, we applied a convenient approach to synthesize graphene-based nanocomposite AMG with about one adenine group per 53 carbon atoms on a graphene sheet and improved electronic conductivity compared with RGO, which has a higher supercapacitor value compared with RGO sheets. The AMG, being a supercapacitor electrode material, has a high discharge capacity and good cycle life.

■ ASSOCIATED CONTENT

Ⓢ Supporting Information

XPS spectra of N1s and O1s, cyclic voltammograms of the product. . This material is available free of charge via the Internet at http://pubs.acs.org.

■ AUTHOR INFORMATION

Corresponding Author

*E-mail: hqcao@mail.tsinghua.edu.cn.

■ ACKNOWLEDGMENTS

The authors are grateful for financial support from the National High Technology Research and Development Program ("863" Program) of China (2012AA030306), the National Natural Science Foundation of China (Nos. 20921001 and 20535020), the Innovation Method Fund of China (No. 20081885189), the National High Technology Research and Development Program of China (No. 2009AA03Z321), and the Natural Science Foundation of Jiangsu Province (No. BK2006717).

■ REFERENCES

(1) Novoselov, K. S.; Geim, A. K.; Morozov, S. V.; Jiang, D.; Zhang, Y.; Dubonos, S. V.; Grigorieva, I. V.; Firsov, A. A. *Science* **2004**, *306*, 666−669.

(2) (a) Stankovich, S.; Dikin, D. A.; Dommett, G. H. B.; Kohlhaas, K. M.; Zimney, E. J.; Stach, E. A.; Piner, R. D.; Nguyen, S. T.; Ruoff, R. S. *Nature* **2006**, *442*, 282−286. (b) Wang, X.; Li, X.; Zhang, L.; Yoon, Y.; Weber, P. K.; Wang, H.; Guo, J.; Dai, H. *Science* **2009**, *324*, 768−771. (c) Geim, A. K; Novoselov, K. S. *Nat. Mater.* **2007**, *6*, 183−191. (d) Park, S.; Ruoff, R. S. *Nat. Nanotechnol.* **2010**, *4*, 217−224. (e) Patil, A. J.; Vickery, J. L.; Scott, T. B.; Mann, S. *Adv. Mater.* **2009**, *21*, 3159−3164. (f) Liu, Z.; Robinson, J. T.; Sun, Z.; Dai, H. *J. Am. Chem. Soc.* **2008**, *130*, 10876−10877. (g) Liu, J.; Fu, S.; Yuan, B.; Li, Y.; Deng, Z. *J. Am. Chem. Soc.* **2010**, *132*, 7279−7281. (h) Dreyer, D. R.; Ruoff, R. S.; Bielawski, C. W. *Angew. Chem., Int. Ed.* **2010**, *49*, 9336−9344.

(3) (a) Dkin, D. A.; Stankovich, S.; Zimney, E. J.; Piner, R. D.; Dommett, G. H. B.; Evmenenko, G.; Nguyen, S. T.; Ruoff, R. S. *Nature* **2007**, *448*, 457−460. (b) Mohanty, N.; Berry, V. *Nano Lett.* **2008**, *8*, 4469−4476. (c) Ramanathan, T.; Abdala, A. A.; Stankovich, S.; Dikin, D. A.; Herrera-Alonso, M.; Piner, R. D.; Adamson, D. H.; Schniepp, H. C.; Chen, X.; Ruoff, R. S.; Nguyen, S. T.; Aksay, I. A.; Prud'Homme, R. K.; Brinson, L. C. *Nat. Nanotechnol.* **2008**, *3*, 327−331. (d) Li, B.; Cao, H.; Shao, J.; Zheng, H.; Lu, Y.; Yin, J.; Qu, M. *Chem. Commun.* **2011**, *47*, 3159−3161. (e) Li, B.; Cao, H.; Shao, J.; Li, G.; Qu, M.; Yin, G. *Inorg. Chem.* **2011**, *50*, 1628−1632. (f) Li, B.; Cao, H.; Shao, J.; Qu, M.; Warner, J. H. *J. Mater. Chem.* **2011**, *21*, 5069−5075.

(4) Gómez-Navarro, C.; Thomas, R.; Bittner, A. M.; Scolari, M.; Mews, A.; Burghard, M.; Kern, K. *Nano Lett.* **2007**, *7*, 3499−3503.

(5) (a) Aricò, A. S.; Bruce, P.; Scrosati, B.; Tarascon, J.-M.; van Schalkwijk, W. *Nat. Mater.* **2005**, *4*, 366−377. (b) Taberna, P. L.; Mitra, S.; Poizot, P.; Simon, P.; Tarascon, J.-M. *Nat. Mater.* **2006**, *5*, 567−573. (c) Simon, P.; Gogotsi, Y. *Nat. Mater.* **2008**, *7*, 845−854.

(6) (a) Yan, S.; Feng, X.; Ivanovici, S.; Müllen, K. *Angew. Chem., Int. Ed.* **2010**, *49*, 8408−8411. (b) Yang, S.; Feng, X.; Wang, L.; Tang, K.; Maier, J.; Müllen, K. *Angew. Chem.,Int. Ed.* **2010**, *49*, 4795−4799.

(c) Stoller, M. D.; Park, S.; Zhu, Y.; An, J.; Ruoff, R. S. *Nano Lett.* **2008**, *8*, 3498−3502.
(7) Hummers, W. S.; Offeman, R. E. *J. Am. Chem. Soc.* **1958**, *80*, 1339−1339.
(8) (a) Liu, Z. F.; Liu, Q.; Huang, Y.; Ma, Y. F.; Yin, S. G.; Zhang, X. Y.; Sun, W.; Chen, Y. S. *Adv. Mater.* **2008**, *20*, 3924−3930. (b) Cote, L. J.; Kim, F.; Huang, J. X. *J. Am. Chem. Soc.* **2009**, *131*, 1043−1049.
(9) Xu, Y. F.; Liu, Z. B.; Zhang, X. L.; Wang, Y.; Tian, J. G.; Huang, Y.; Ma, Y. F.; Zhang, X. Y.; Chen, Y. S. *Adv. Mater.* **2009**, *21*, 1275−1279.
(10) Boukhvalov, D. W.; Katsnelson, M. I. *J. Am. Chem. Soc.* **2008**, *130*, 10697−10701.
(11) Li, X.; Zhang, G.; Bai, X.; Sun, X.; Wang, X.; Wang, E.; Dai, H. *Nat. Nanotechnol.* **2008**, *3*, 538−542.
(12) Luo, Z. T.; Lu, Y.; Somers, L. A.; Johnson, A. T. C. *J. Am. Chem. Soc.* **2009**, *131*, 898−899.
(13) Xu, Y. F.; Liu, Z. B.; Zhang, X. L.; Wang, Y.; Tian, J. G.; Huang, Y.; Ma, Y. F.; Zhang, X. Y.; Chen, Y. S. *Adv. Mater.* **2009**, *21*, 1275−1279.
(14) Park, S.; Lee, K. S.; Bozoklu, G.; Cai, W.; Nguyen, S. T.; Ruoff, R. S. *ACS Nano.* **2008**, *2*, 572−578.
(15) Guo, P.; Song, H. H.; Chen, X. H. *Electrochem. Commun.* **2009**, *11*, 1320−1324.
(16) (a) In *Raman spectroscopy in carbons: from nanotubes to diamond*; Ferrari, A. C., Robertson, J., Eds.; The Royal Society: London, 2004. (b) Elias, D. C.; Nair, R. R.; Mohiuddin, T. M. G.; Morozov, S. V.; Blake, P.; Halsall, M. P.; Ferrari, A. C.; Boukhvalov, D. W.; Katsnelson, M. I.; Geim, A. K.; Novoselov, K. S. *Science* **2009**, *323*, 610−613. (c) Chen, C.-F.; Park, C.-H.; Boudouris, B. W.; Horng, J.; Geng, B.; Girit, C.; Zettl, A.; Crommie, M. F.; Segalman, R. A.; Louie, S. G.; Wang, F. *Nature* **2011**, *471*, 617−620.
(17) Rao, C. N. R.; Sood, A. K.; Subrahmanyam, K. S.; Govindaraj, A. *Angew. Chem., Int. Ed.* **2009**, *48*, 7752−7777.
(18) Ferrari, A. C.; Meyer, J. C.; Scardaci, V.; Casiraghi, C.; Lazzeri, M.; Mauri, F.; Piscanec, S.; Jiang, D.; Novoselov, K. S.; Roth, S.; Geim, A. K. *Phys. Rev. Lett.* **2006**, *97* (187401), 1−4.
(19) (a) Rao, A. M.; Eklund, P. C.; Bandow, S.; Thess, A.; Smalley, R. E. *Nature* **1997**, *388*, 257−259. (b) Su, Q.; Pang, S.; Alijani, V.; Li, C.; Feng, X.; Mülen, K. *Adv. Mater.* **2009**, *21*, 3191−3195.
(20) Jiao, L.; Wang, X.; Diankov, G.; Wang, H.; Dai, H. *Nat. Nanotechnol.* **2010**, *5*, 321−325.
(21) Mattevi, C.; Eda, G.; Agnoli, S.; Miller, S.; Mkhoyan, K. A.; Celik, O.; Mostrogiovanni, D.; Granozzi, G.; Garfunkel, E.; Chhowalla, M. *Adv. Funct. Mater.* **2009**, *19*, 2577−2583.
(22) Graf, D.; Molitor, F.; Enssin, K.; Stampfer, C.; Jungen, A.; Hierold, C.; Wirtz, L. *Nano Lett.* **2007**, *7*, 238−242.
(23) Gupta, A.; Chen, G.; Joshi, P.; Tadigadapa, S.; Eklund, P. C. *Nano Lett.* **2006**, *6*, 2667−2673.
(24) Das, A.; Pisana, S.; Chakraborty, B.; Piscanec, S.; Saha, S. K.; Waghmare, U. V.; Novoselov, K. S.; Krishnamurthy, H. R.; Geim, A. K.; Ferrari, A. C.; Sood, A. K. *Nat. Nanotechnol.* **2008**, *3*, 210−215.
(25) McAllister, M. J.; Li, J. L.; Adamson, D. H.; Schniepp, H. C.; Abdala, A. A.; Liu, J.; Herrera-Alonso, M.; Milius, D. L.; Car, R.; Prud'homme, R. K.; Aksay, I. A. *Chem. Mater.* **2007**, *19*, 4396−4404.
(26) Jeong, H. K.; Lee, Y. P.; Lahaye, R. J. W. E.; Park, M. H.; An, K. H.; Kim, I. J.; Yang, C. W.; Park, C. Y.; Ruoff, R. S.; Lee, Y. H. *J. Am. Chem. Soc.* **2008**, *130*, 1362−1366.
(27) Wei, D. C.; Liu, Y. Q.; Zhang, H. L.; Huang, L. P.; Wu, B.; Chen, J. Y.; Yu, G. *J. Am. Chem. Soc.* **2009**, *131*, 11147−11154.
(28) Zhang, W. X.; Cui, J. C.; Tao, C. A.; Wu, Y. G.; Li, Z. P.; Ma, L.; Wen, Y. Q.; Li, G. T. *Angew.Chem., Int. Ed.* **2009**, *48*, 5864−5868.
(29) Furukawa, M.; Yamada, T.; Katano, S.; Kawai, M.; Ogasawara, H.; Nilsson, A. *Surf. Sci.* **2007**, *601*, 5433−5440.
(30) Zhuang, X.-D.; Chen, Y.; Liu, G.; Li, P.-P.; Zhu, C.-X.; Kang, E.-T.; Neoh, K.-G.; Zhang, B.; Zhu, J.-H.; Li, Y.-X. *Adv. Mater.* **2010**, *22*, 1731−1735.
(31) Zhang, L.-S.; Liang, X.-Q.; Song, W.-G.; Wu, Z.-Y. *Phys. Chem. Phys. Chem.* **2010**, *12*, 12055−12059.
(32) Hontoria-Lucas, C.; López-Peinado, A. J.; López-González, J. D. D.; Rojas-Cervantes, M. L.; Matín-Aranda, R. M. *Carbon* **1995**, *33*, 1585−1592.
(33) Zhang, G.; Sun, S.; Yang, D.; Dodelet, J.-P.; Sacher, E. *Carbon* **2008**, *46*, 196−205.
(34) Xu, Y.; Bai, H.; Lu, G.; Li, C.; Shi, G. *J. Am. Chem. Soc.* **2008**, *130*, 5856−5857.
(35) Rao, C. N. R.; Müller, A. Cheetham, A. K. *Nanomaterials chemistry—recent developments and new directions*; Wiley-VCH Verlag GmbH & Co. KGaA: Weinheim, Germany, 2007.
(36) Miller, J. R.; Outlaw, R. A.; Holloway, B. C. *Science* **2010**, *329*, 1637−1639.
(37) Chmiola, J.; Yushin, G.; Gogotsi, Y.; Portet, C.; Simon, P.; Taberna, P. L. *Science* **2006**, *313*, 1760−1763.
(38) Bard, A. J. Faulkner, L. R. *Electrochemical Methods Fundamentals and Applications*, 2nd ed.; John Wiley & Sons, Inc.: New York, 2001.
(39) Fusalba, F.; Mehdi, N.; El.; Breau, L.; Bélanger, D. *Chem. Mater.* **1999**, *11*, 2743−2753.
(40) (a) Conway, B. E. *Electrochemical supercapacitors: scientific fundamentals and technological applications*; Kluwer Academic/Plenum Publishers: New York, 1999. (b) Jeong, H.-K.; Jin, M.; Ra, E. J.; Sheem, K. Y.; Han, G. H.; Arepalli, S.; Lee, Y. H. *ACS Nano* **2010**, *4*, 1162−1166.
(41) Wu, K.; Fei, J.; Bai, W.; Hu, S. *Anal. Bioanal. Chem.* **2003**, *376*, 205−209.
(42) Yu, C.; Masarapu, C.; Rong, J.; Wei, B.; Jiang, H. *Adv. Mater.* **2009**, *21*, 4793−4797.
(43) Jiang, J.; Liu, J.; Ding, R.; Zhu, J.; Li, Y.; Hu, A.; Li, X.; Huang, X. *ACS Appl. Mater. Interface* **2010**, *3*, 99−103.
(44) Li, Y.; Zhao, X.; Xu, Q.; Zhang, Q.; Chen, D. *Langmuir* **2011**, *27*, 6458−6463.
(45) Zhang, X.; Shi, W.; Zhu, J.; Kharistal, D. J.; Zhao, W.; Lalia, B. S.; Hng, H. H.; Yan, Q. *ACS Nano* **2011**, *5*, 2013−2019.
(46) Kim, J.-H.; Zhu, K.; Yan, Y.; Perkins, C. L.; Frank, A. J. *Nano Lett.* **2010**, *10*, 4099−4104.
(47) Yuan, C.; Zhang, X.; Su, L.; Gao, B.; Shen, L. *J. Mater. Chem.* **2009**, *19*, 5772−5777.
(48) Xia, X.-H.; Tu, J.-P.; Wang, X.-L.; Gu, C.-D.; Zhao, X.-B. *J. Mater. Chem.* **2011**, *21*, 671−679.
(49) Wei, T.-Y.; Chen, C.-H.; Chien, H.-C.; Lu, S.-Y.; Hu, C.-C. *Adv. Mater.* **2010**, *22*, 347−351.
(50) Deng, M. G. *Supercapacitor: research on electrode materials*; University of Science and Technology of China Press: Hefei, China, 2009.
(51) Wang, D.-W.; Li, F.; Zhao, J.; Ren, W.; Chen, Z.-G.; Tan, J.; Wu, Z.-S.; Gentle, I.; Lu, G. Q.; Cheng, H.-M. *ACS Nano* **2009**, *3*, 1745−1752.
(52) Kim, Y.-T.; Mitani, T. J. *Power Sources* **2006**, *158*, 1517−1522.
(53) Tang, H.; Chen, L.; Xing, C.; Guo, Y.-G.; Wang, S. *Macromol. Rapid Commun.* **2010**, *31*, 1892−1896.